

OH PLIF Visualization of the UVa Supersonic Combustion Experiment: Configuration C

Colin D. McRae¹, Craig T. Johansen²
University of Calgary, Calgary, AB, T2N 1N4

Paul M. Danehy³
NASA Langley Research Center, Hampton, VA, 23681-2199

Emanuela C.A. Gallo⁴, Luca M.L. Cantu⁵, Gaetano Magnotti⁶, Andrew D. Cutler⁷
The George Washington University, Newport News, VA, 23602

Robert D. Rockwell, Jr.⁸, Christopher P. Goyne⁹, James C. McDaniel¹⁰
University of Virginia, Charlottesville, VA, 22904

Non-intrusive hydroxyl radical (OH) planar laser-induced fluorescence (PLIF) measurements were obtained in configuration C of the University of Virginia supersonic combustion experiment. The combustion of hydrogen fuel injected through an unswept compression ramp into a supersonic cross-flow was imaged over a range of streamwise positions. Images were corrected for optical distortion, variations in the laser sheet profile, and different camera views. Results indicate an effect of fuel equivalence ratio on combustion zone shape and local turbulence length scale. The streamwise location of the reaction zone relative to the fuel injector was also found to be sensitive to the fuel equivalence ratio. The flow boundary conditions in the combustor section, which are sensitive to the fuel flow rate, are believed to have caused this effect. A combination of laser absorption and radiative trapping effects are proposed to have caused asymmetry observed in the images. The results complement previously published OH PLIF data obtained for configuration A along with other non-intrusive measurements to form a database for computational fluid dynamics (CFD) model validation.

I. Introduction

SCRAMJET engine research has become increasingly reliant on non-intrusive flow measurement techniques over conventional probes to build validation datasets for computational fluid dynamics (CFD) models. Model validation is a key step in the development of numerical design tools since the interaction between turbulence, chemistry, and shock wave propagation in supersonic flows is not well understood. Validated numerical models can be used as efficient design tools and with optimization routines to improve hypersonic aerospace propulsion technology. Laser diagnostics, in particular, can be used to extract both qualitative visualization data and quantitative flow property information. Quantitative techniques are often limited by operating conditions, facility design, and the type of data that can be acquired. Therefore, a complete experimental validation dataset requires several measurement techniques performed in a ground-test facility where operating conditions and flow geometry

¹ Graduate Student, Department of Mechanical and Manufacturing Engineering, Member AIAA.

² Assistant Professor, Department of Mechanical and Manufacturing Engineering, Member AIAA.

³ Research Scientist, Advanced Sensing and Optical Measurement Branch, MS 493, Associate Fellow AIAA.

⁴ Doctoral Student, Department of Mechanical and Aerospace Engineering, Member AIAA.

⁵ Doctoral Student, Department of Mechanical and Aerospace Engineering, Member AIAA.

⁶ Doctoral Student, Department of Mechanical and Aerospace Engineering, Member AIAA.

⁷ Professor, Department of Mechanical and Aerospace Engineering, Associate Fellow AIAA.

⁸ Senior Scientist, Department of Mechanical and Aerospace Engineering, Member AIAA.

⁹ Research Associate Professor, Department of Mechanical and Aerospace Engineering, Associate Fellow AIAA.

¹⁰ Professor, Department of Mechanical and Aerospace Engineering, Associate Fellow AIAA.

can be varied systematically. The National Center for Hypersonic Combined Cycle Propulsion (NCHCCP) has organized a series of ground-based experiments to further understand the flow field associated with a dual-mode scramjet engine. This engine incorporates both a subsonic and supersonic combustion mode into a single design in order to simulate mode transition. The University of Virginia Scramjet Combustion Facility (UVaSCF) allows variable engine configurations, variable fuel types, and supports a host of non-intrusive optical diagnostics. The diagnostics include focused schlieren,¹ stereoscopic particle image velocimetry (SPIV),¹ tunable diode laser absorption spectroscopy (TDLAS),² tunable diode laser absorption tomography (TDLAT),³ coherent anti-Stokes Raman spectroscopy (CARS),⁴ and hydroxyl radical (OH) planar laser-induced fluorescence (PLIF).⁵

This paper reports on OH PLIF visualization data obtained for a new hydrogen fuel combustor configuration and compares results to previous work.⁵ To first order, OH PLIF images provide spatially correlated concentration distributions of combustion radicals in the flow.⁶ Although OH persists outside of the reaction zone, the distribution of OH represents the overall shape of the combustion front. Several factors limit the concentration measurements to being qualitative. First, the fluorescence signal is sensitive to local flow field properties such as temperature, pressure, and concentrations of major species. Collisional quenching, whereby excited molecules dissipate energy through collisions rather than through spontaneous emission, is an example of a mechanism that causes this sensitivity. Second, optical density effects can decrease signal-to-noise levels and introduce systematic bias errors. Laser absorption, for example, causes an artificial reduction in fluorescence signal intensity in the direction of the laser beam. This occurs in optically dense media where a portion of the laser energy is lost due to absorption, leaving less incident laser energy to excite subsequent molecules. Radiative trapping occurs in optically dense media where spontaneously emitted photons from excited molecules are reabsorbed by neighboring molecules.⁷ There are techniques that can reduce optical density effects. For example, it is possible to make quantitative measurements of OH PLIF using a KrF excimer laser with a higher pulse energy to excite ($v'=3, v''=0$) vibronic transitions where optical density effects can be significantly reduced.^{8,9} Visualization data, however, are easier to acquire and still provide useful information about reactions occurring in the flow field, flow field structures and combustion front shape.

II. Facility and PLIF Setup

The UVaSCF is a vertically oriented direct-connect scramjet combustor apparatus designed to simulate Mach 5 flight enthalpy.⁴ An electrically heated tank provides pressurized air to a nozzle that accelerates the air to Mach 2 into the scramjet test section.

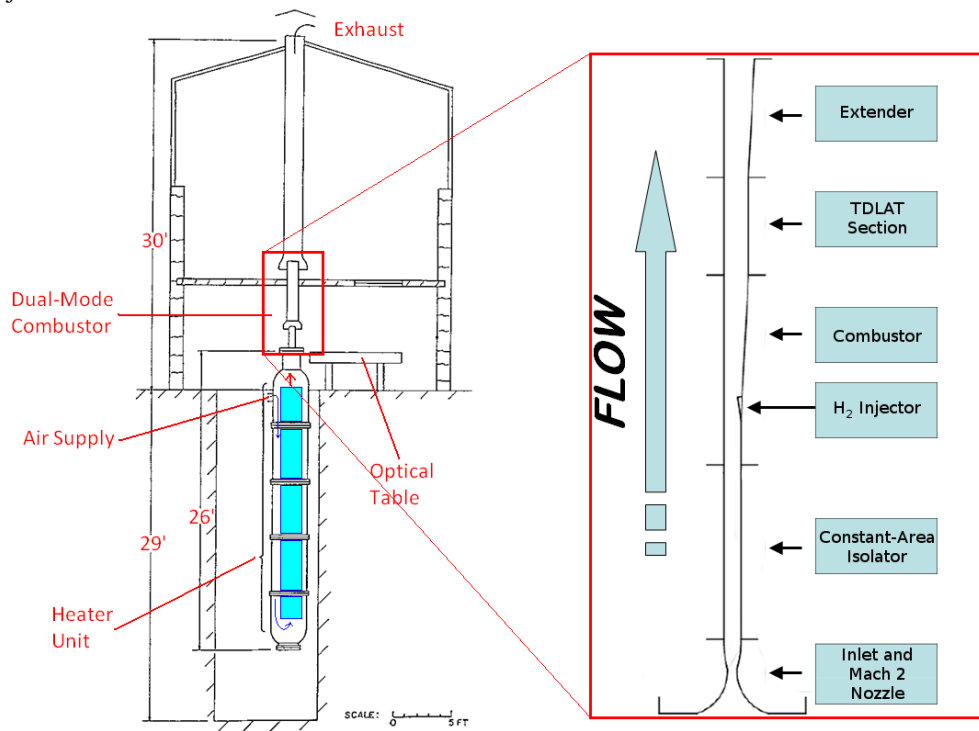


Figure 1. UVaSCF with complete test section configuration.

Figure 1 shows a schematic of the test section complete with all modular sections, an arrangement which is denoted as configuration C. It consists of a constant area isolator with a 25.4 mm × 38.1 mm (1 in. × 1.5 in.) cross-section, a combustor with an expanding cross-section, a constant area TDLAT section, and an expanding extender section. Gas exits the extender into an exhaust duct that vents from the top of the building. The modular nature of the facility allows for different configurations to be tested. A recent paper reported OH distributions in configuration A (top panel in Fig. 2), which does not include the isolator or TDLAT sections.⁵ In the current study, configuration C was used, shown in the bottom panel in Fig. 2. Similar to the configuration A tests, the stagnation pressure was 300 kPa and the stagnation temperature was 1200 K. In the combustor section, a single, unswept, compression ramp injector is mounted to the wall. The ramp is oriented at 7.1 degrees relative to the freestream flow and 10 degrees relative to the injector wall. The injector interior is conical with a converging-diverging nozzle. Hydrogen fuel is accelerated to approximately Mach 1.7 at the injector exit plane. The injector wall in the combustor diverges at an angle of 2.9 degrees. This same angle of divergence occurs in the extender section. The hydrogen fuel equivalence ratio, ϕ , is a relative measure of the concentration of OH in the combustor. For the results presented, two fuel equivalence ratios were used: a low fuel equivalence ratio of $\phi=0.18$ and a high fuel equivalence ratio of $\phi=0.49$. In the configuration A tests, $\phi=0.17$ and $\phi=0.34$ were used.⁵

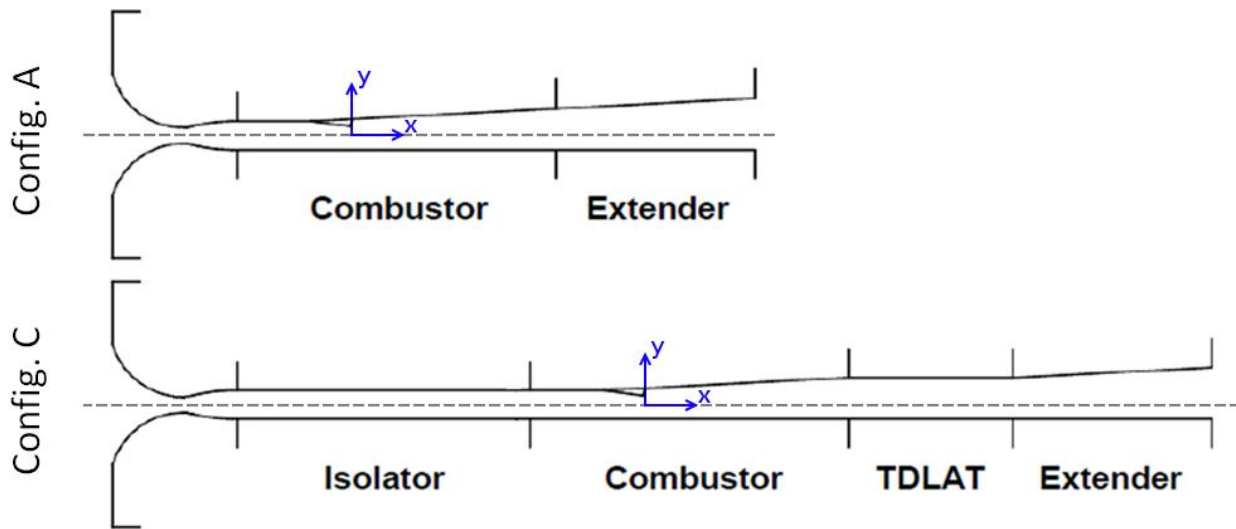


Figure 2. Modular configurations of the UVaSCF. Configuration C is used in the current study.

The PLIF setup is identical to that used in the previous configuration A experiments.⁵ An injection-seeded Nd:YAG laser was frequency doubled to 532 nm to pump a Spectra Physics PDL-2 dye laser. The 567.1 nm output was then frequency doubled resulting in tunable light near 283.55 nm with an 8 ns pulse width. This was used to excite a relatively temperature insensitive $Q_1(8)$ transition of OH. Based on a similar scramjet experiment using this transition, the fluorescence intensity was expected to vary with temperature by less than 20% over a range of temperatures from 1300 K to 3000 K.¹⁰ A series of UV mirrors relayed the beam from the mobile laser cart onto a motorized translation stage. The beam was expanded in one direction with a UV cylindrical lens ($f = 25$ mm) and then collimated in the horizontal direction with a UV spherical lens (50 mm diameter, $f = 250$ mm). In the vertical direction (perpendicular to the flow axis), this spherical lens forms the laser beam into a <1 mm thick sheet. Optical access into the combustor section was facilitated by two UV grade fused silica windows mounted on the side walls. The laser sheet entered from one side of the duct and was viewed by a camera from the other side. A schematic of the optical table setup is shown in Fig. 3.

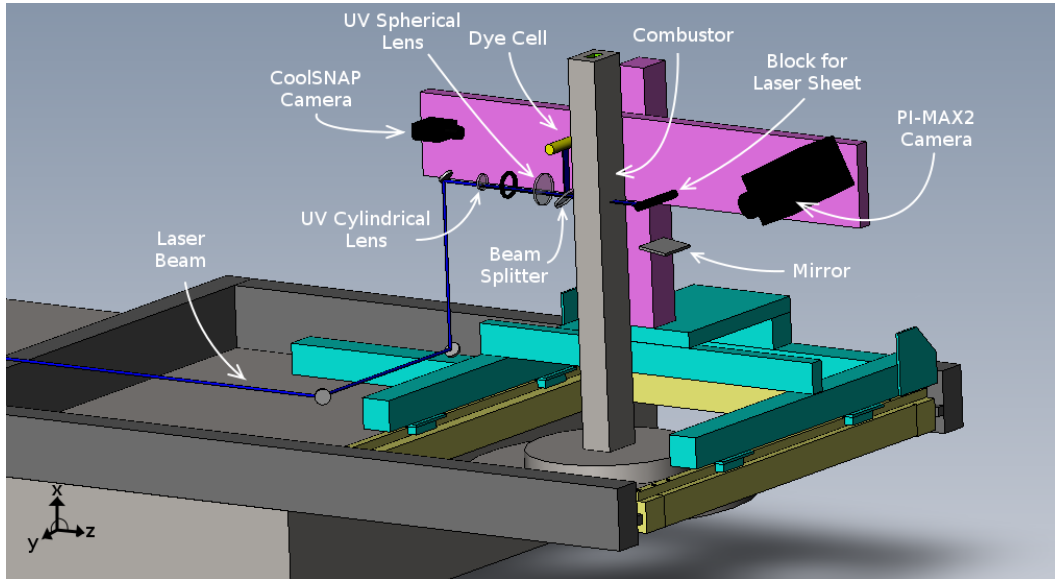


Figure 3. Schematic of translating PLIF system for UVaSFC.

The experimental setup is shown in Fig. 4. The 50 mm wide and less than 1 mm thick laser sheet was directed perpendicular to the flow direction. An intensified charge-coupled device (ICCD) PI-MAX2 camera (512×512 pixel array) viewed the image plane via a mirror located near the duct, allowing a more perpendicular view of the sheet than would have been possible with a direct camera view of the sheet. The camera used a SB Gen II intensifier and acquired images at 10 Hz though the laser operated at 20 Hz. A CoolSNAP laser sheet-profiling camera captured laser intensity fluctuations from a Rhodamine filled dye cell. A beam splitter was placed between the test section and spherical lens to redirect a portion of the laser sheet light into the dye cell. The PI-MAX2 and CoolSNAP cameras were synchronized so that the laser sheet profile could be used to correct the PLIF data on a shot-by-shot basis. All of the following were attached to a motorized traverse system: laser sheet forming optics, PI-MAX2 camera and viewing mirrors, dye cell and CoolSNAP sheet-profiling camera. Translating these components vertically allowed for different streamwise positions in the cross-plane to be imaged.

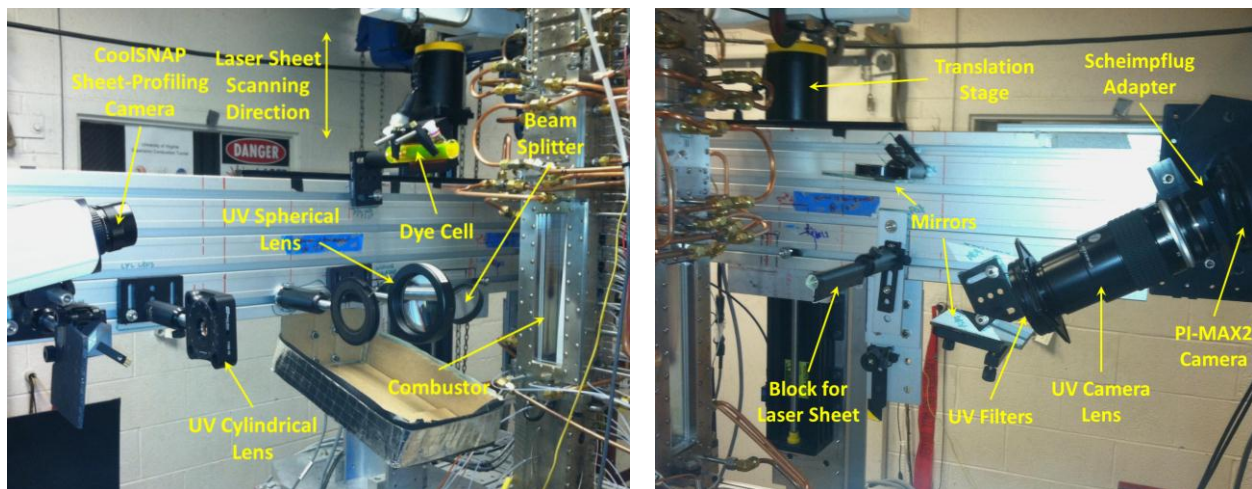


Figure 4. Left and right views of experimental setup. The equipment is shown in the configuration for camera view 2 and translated away from the actual imaging position.

To be consistent with previously reported results,^{4,5,11,12} the PLIF images herein are reported using a non-dimensionalized reference system relative to the compression ramp height, $H = 6.35$ mm (0.25 in.). Measurements were focused on three measurement dwell positions ($x/H = 6, 12,$ and 18), though additional measurements were also obtained. In this coordinate system, $x/H = 0$ refers to the base of the fuel injector. Physical constraints of the

translation stage and facility geometry required the use of two different camera configurations to image the full range of streamwise positions in the combustor (Fig. 5). Camera view 1 covers the range from $x/H = 23.7$ to $x/H = 6$. Camera view 2 covers the range from $x/H = 6$ to $x/H = -10.5$. Note that camera views 1 and 2 imaged the laser sheet from opposite perspectives. Camera view 1 imaged the laser sheet from the upstream side, pointed downstream through the flow. Camera view 2 imaged the sheet from the downstream side, pointed upstream through the flow. While this would normally require a mirror correction in post-processing to properly synchronize the views between the two camera configurations, the use of the extra physical mirror in camera view 2 naturally corrected the issue. However, the different optical paths for each camera view resulted in different perspective distortions, spatial resolutions, and radiative trapping bias errors for each camera view. This is discussed in the *Results* section below.

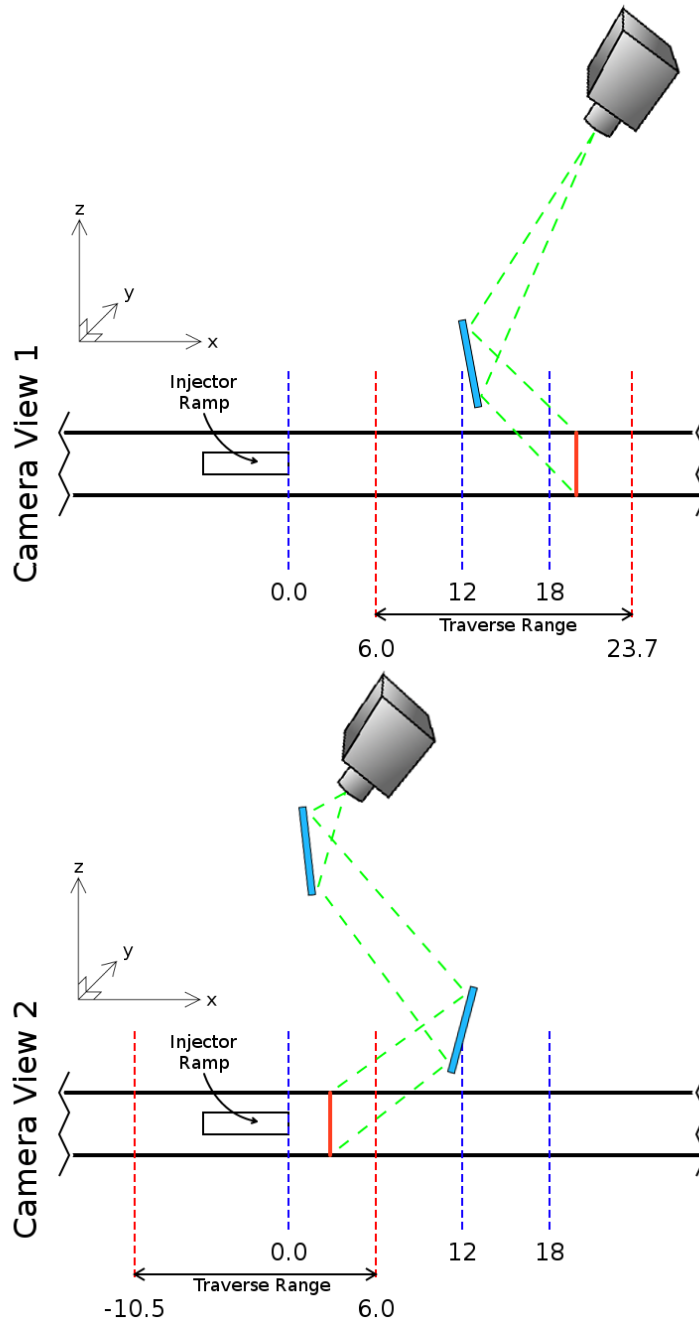


Figure 5. Camera views used to cover total streamwise range in combustor. Values are displayed in non-dimensionalized units (x/H). Note the $+y$ direction is into the page and injector ramp is on $+y$ side of duct.

III. Image Processing

Four major steps are involved in processing of the PLIF images to correct for optical distortions and camera perspective. These include background subtraction, image unwarping, laser sheet correction, and synchronization between camera views and runs. With the exception of natural emission corrections, the steps are the same as those described in the post-processing of configuration A images⁵ and are based on the procedure outlined by Danehy *et al.* for nitric oxide (NO) PLIF.¹³ The unwarping procedure involves imaging a dotcard, which is a grid of uniform square dots printed on a white card stock, placed in the plane of the laser sheet. The dots are equally spaced at 3.175 mm apart, allowing for determination of the spatial resolution of the images. The image processing software, ImageJ,¹⁴ was used with the dotcard images to calculate a correction matrix for each camera view. This was applied to all image data obtained from the PI-MAX2 camera to produce images without distortion (i.e., effectively normal to the laser sheet). The spatial resolution after image unwarping was 12.6 ± 0.1 pixels/mm. The images were subsequently scaled so that each set has a magnification equivalent to that of configuration A, or 11.85 pixels/mm.

The background correction procedure used with configuration A images involved subtracting a constant background signal from the entire set of images for each run.⁵ The magnitude of the background signal level was determined from a 2000-shot average in a region of the image without PLIF signal. In the current study, an alternative background correction was applied using natural emission images obtained with the facility running but without laser excitation. These images captured flow luminosity at different streamwise positions and for both fuel equivalence ratios. Figure 6 shows a raw single-shot PLIF image and the corresponding (100-shot averaged) luminosity background image. It is clear that the luminosity is non-uniform in the vertical (y) direction, so a single-value background subtraction cannot accurately correct for the natural luminosity of the flow.

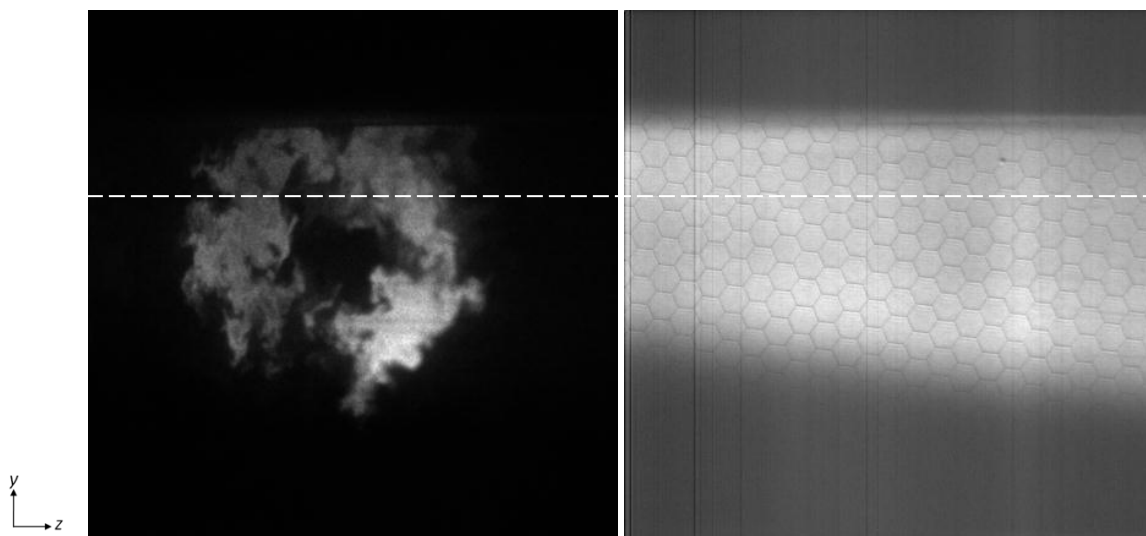


Figure 6. Raw single-shot PLIF image (left) and corresponding averaged luminosity image (right) for camera view 1 at $x/H=12$ and $\phi=0.18$. Images have arbitrary intensity scaling. Dashed line indicates location of line plots in Fig. 7.

The white dashed line across Fig. 6 indicates the location of the signal intensity line-plots shown in Fig. 7. Also included in Fig. 7 is a line-plot of background signal intensity based on images without the facility or laser system operating. The flow luminosity, which varied between 160 and 410 signal counts, includes the constant background signal (approximately 124 signal counts). In cases where the laser sheet was translated between measurement dwell positions and luminosity images were unavailable, an interpolation algorithm was used to construct the luminosity images at intermediate streamwise positions. The luminosity images were used in place of a constant background signal for the background subtraction.

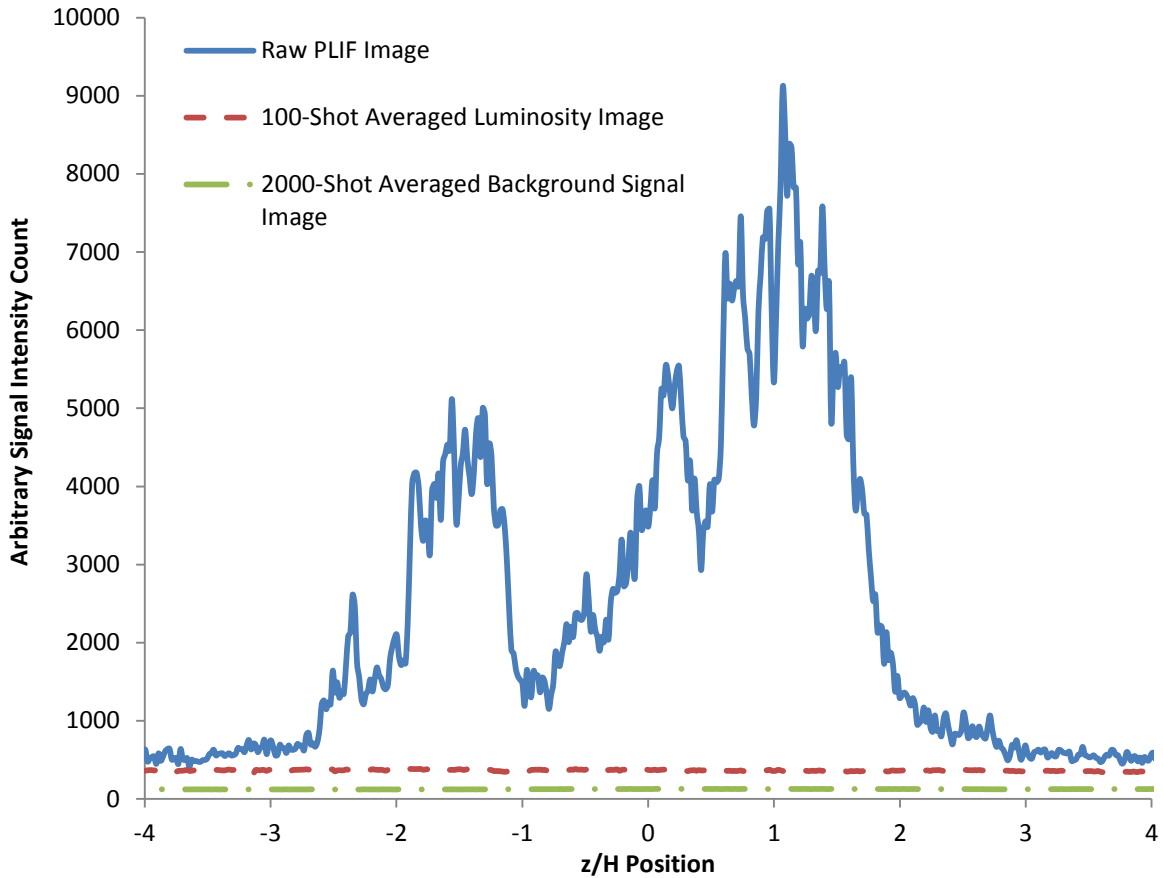


Figure 7. Line plots showing signal comparison of raw PLIF image, luminosity image, and background noise ($x/H=12$, $\phi=0.18$) at a location indicated by the white dashed line in Fig. 6.

The results presented herein have been cropped to the approximate location of the facility walls based on the magnification reported from the configuration A results as discussed above. The images have been rotated such that the ramp injector wall is at the top of the images. In all of the images, the laser sheet direction is from left to right ($+z$) and the downstream direction is into the page ($+x$). Approximate cropping locations are given in Fig. 8 below, indicated by white dashed lines. Configuration A results were cropped such that they included scatter off of the facility walls. The use of an additional filter (Semrock FF01-320/40-25, centered at 320 nm with a 40 nm bandpass, 25 mm diameter) in configuration C eliminated the majority of laser scatter from the facility walls.

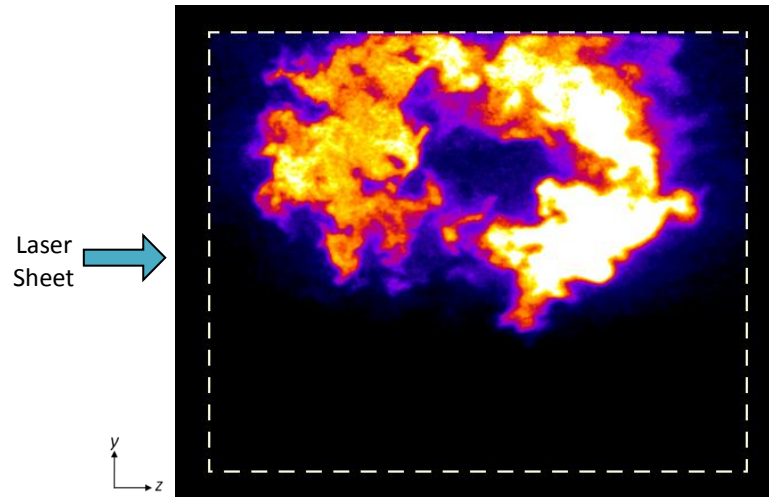


Figure 8. Sample OH PLIF image and approximate location of facility walls (dashed line). $x/H=12$

In some of the corrected images presented below, there are noticeable streaks in the OH PLIF images. This streaking is visible in the uncorrected raw data, ruling out the possibility of being a result of the background subtraction or laser sheet profile corrections applied. The position of the streaks changes with streamwise position, but is consistent in different runs at the same streamwise position indicating that it was caused by physical blockage of the imaging system. This is likely due to dust, contaminants, or scratches on the combustor windows. A low-pass filter correction to eliminate the streaks was not applied to the images as it would degrade image quality away from the streaks. Therefore, the streaks – which are particularly noticeable in the averaged images – were retained in the final processed images.

IV. Results

Figure 9 shows single-shot (left), 2000-shot average (center), and standard deviation (right) images for the three streamwise positions of interest ($x/H = 6, 12, \text{ and } 18$). Hydrogen fuel was injected at an equivalence ratio of $\phi = 0.18$. The images have been processed as described above, approximately cropped at the facility wall locations, and rotated such that the injector ramp wall is at the top of the images. For streamwise positions near the injector, two distinct lobes in the PLIF signal are visible surrounding a dark, fuel-rich region in the center. Moving downstream, away from the injector, the fuel and air mix allowing combustion to occur and the PLIF signal becomes more distributed. The highly turbulent structure of the flow is apparent from the standard deviation images, with strong signal over the entire region of OH concentration. The single-shot images show well-defined turbulent flow structures in the combustion region. Asymmetry of the PLIF signals is discussed in the next section.

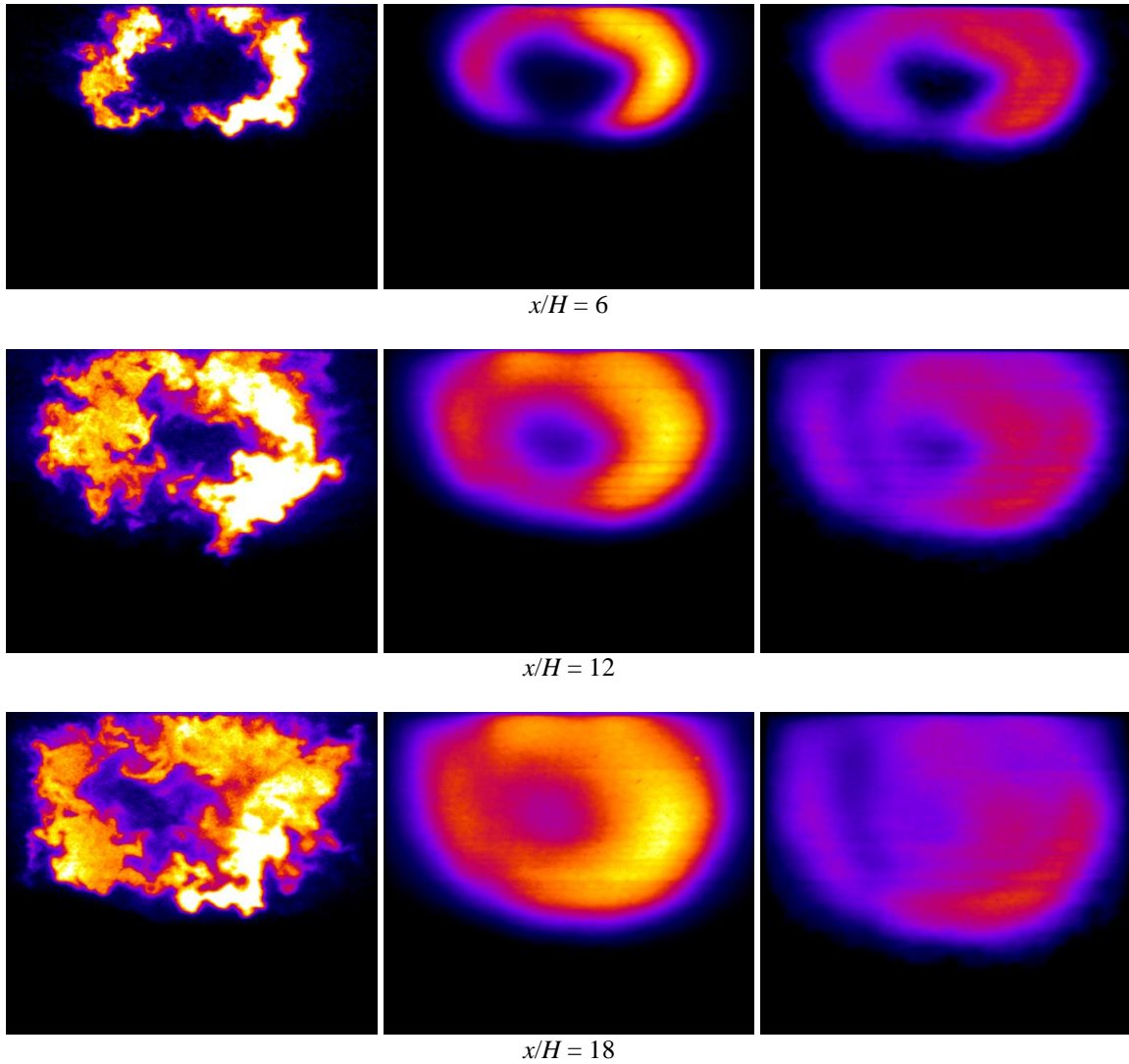


Figure 9. Single-shot (left), average (middle), and standard deviation (right) OH PLIF images for $\phi=0.18$.

Results from the higher fuel equivalence ratio ($\phi = 0.49$) tests are shown in Fig. 10. It appears that the higher mass flow rate of hydrogen results in a reduction in the characteristic turbulence length scale and alters the overall combustion zone shape downstream. There is a larger core region in the center of the jet where the mixture is too rich to burn. The deficit in OH concentration (marking regions of high concentrations of unburnt fuel) at the jet center remains visible, even at the furthest downstream location. In addition, the physical size of the combustion zone appears to increase more rapidly. At the $x/H = 18$ dwell position, PLIF signal is distributed across nearly the entire duct. In contrast, only two-thirds of the duct shows OH concentrations in the lower fuel equivalence ratio case. It is likely that the larger fuel flow rate ($\phi = 0.49$) causes a strong shock wave to form in the flow upstream of the injector, resulting in subsonic flow near the compression ramp. In the lower equivalence ratio tests, this does not occur and the fuel jet interacts with a supersonic cross-flow. This results in an effective change in inflow boundary conditions upstream of the fuel injector. In addition, without the TDLAT section in Configuration A, the back pressure at the exit of the combustor is higher than what is observed in Configuration C. This results in an effective change in outflow boundary conditions at the combustor exit. Therefore, the changes in boundary conditions at the combustor section could result in different flow regimes for each configuration.

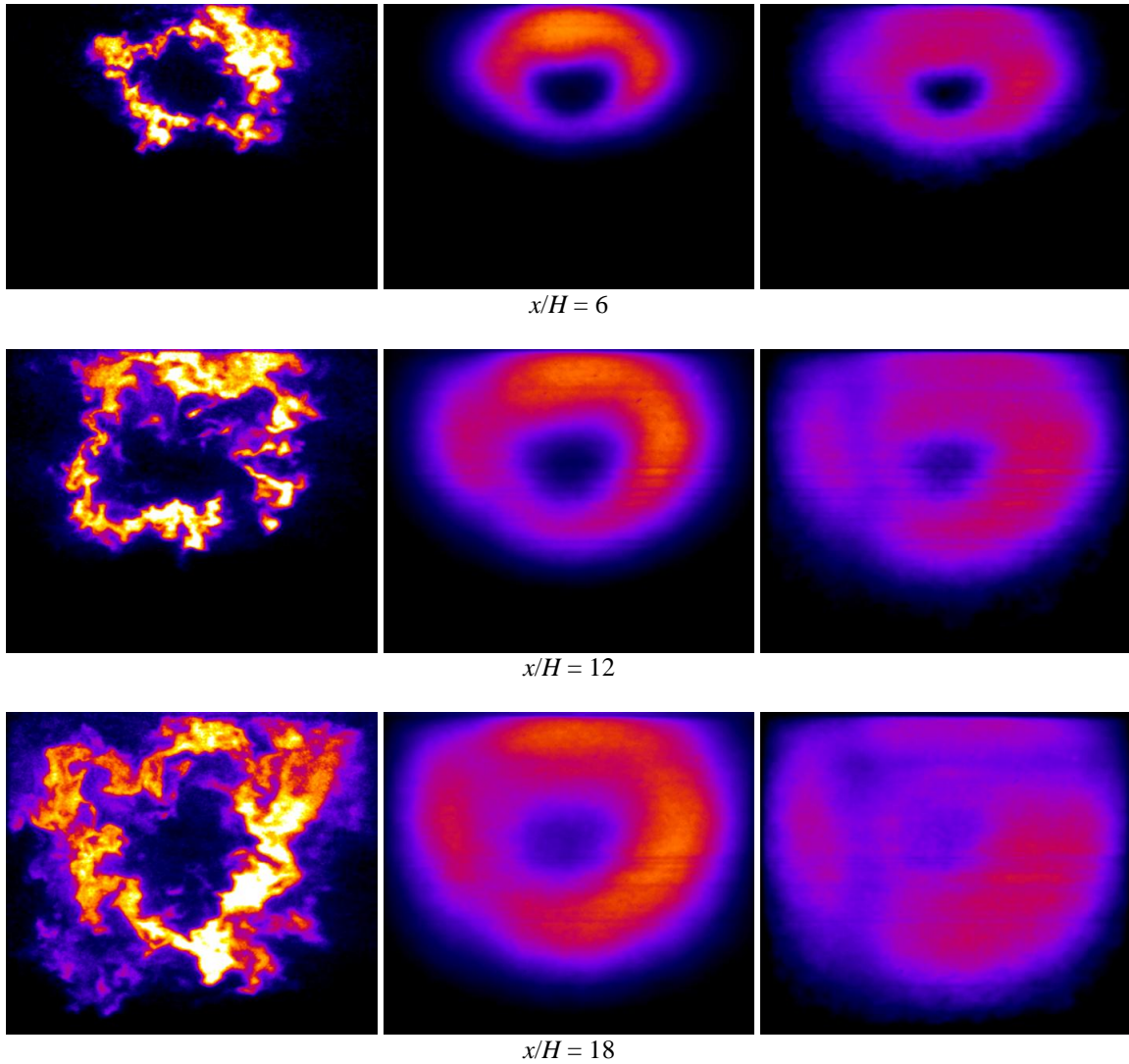


Figure 10. Single-shot (left), average (middle), and standard deviation (right) OH PLIF images for $\phi=0.49$.

Of particular interest in the PLIF visualization data is the combustion behavior near the injector exit plane. Figure 11 and Figure 12 show reconstructed images near the injector for low and high fuel equivalence ratio tests, respectively. The laser sheet was scanned in one millimeter steps from $x/H = 0$ (at the injector) to positions slightly downstream. In the interest of space, only two positions ($x/H = 0$ and 0.6) are reported, and the images have been cropped to a smaller area around the injector. Equivalent arbitrary brightness and contrast settings have been applied to the figures below and they are not correlated to the rest of the results presented herein. Although PLIF signal is visible at the injector face for both cases, it is much stronger (up to four times) in the higher equivalence ratio tests. At $x/H = 0$, the rectangular shape of the injector face is clearly recognizable. In scans over the injector, there is no signal upstream of $x/H = 0$ for both equivalence ratio tests.

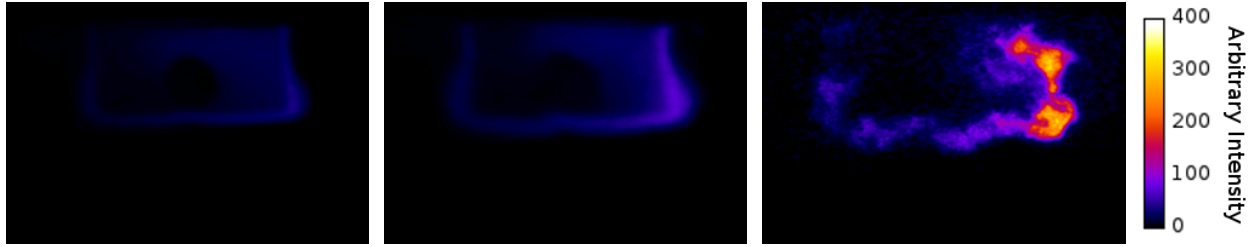


Figure 11. OH distribution near the injector for $\phi=0.18$; averaged image at $x/H = 0$ (left), averaged image at $x/H = 0.6$ (center) and single-shot image at $x/H = 0.6$ (right).

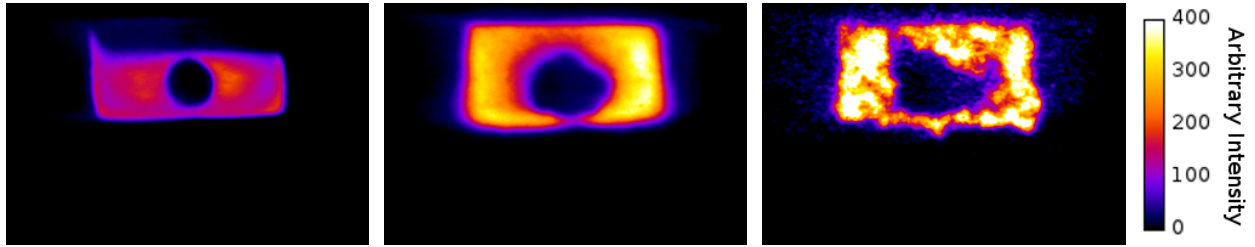


Figure 12. OH distribution near the injector for $\phi=0.49$; averaged image at $x/H = 0$ (left), averaged image at $x/H = 0.6$ (center) and single-shot image at $x/H = 0.6$ (right). Intensity scaling is the same as used in Fig. 11.

To provide a sense of the streamwise distribution of OH and the progression of combustion, single-shot images were overlaid onto a 3D wireframe of the combustor. Figure 13 shows the combustion zone progression for a fuel equivalence ratio $\phi = 0.18$, and Fig. 14 shows the progression for $\phi = 0.49$. The single-shot images are separated by a step size of $3 x/H$, starting from a position of $x/H = 1$ to 22. For the lower fuel equivalence ratio, the confined size of the plume even at far downstream positions is apparent. Conversely, the higher fuel equivalence ratio shows the plume covering nearly the entire combustor cross-section. However, the distribution of OH is much more evenly distributed in the lower fuel equivalence ratio case, especially at the furthest downstream positions. For comparison, Fig. 15 shows corresponding configuration A results for an equivalence ratio of $\phi = 0.17$.

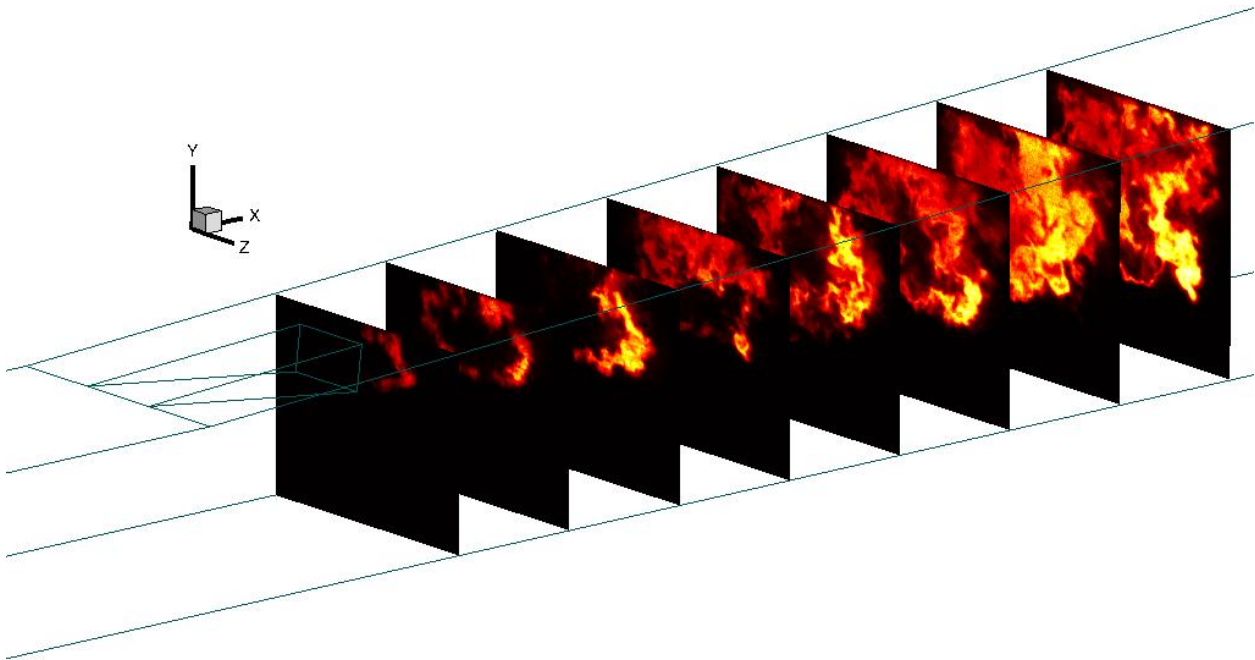


Figure 13. Combustor 3D wireframe drawing with single-shot PLIF overlay showing streamwise distribution from $x/H = 1$ to 22 for $\phi=0.18$. Configuration C.

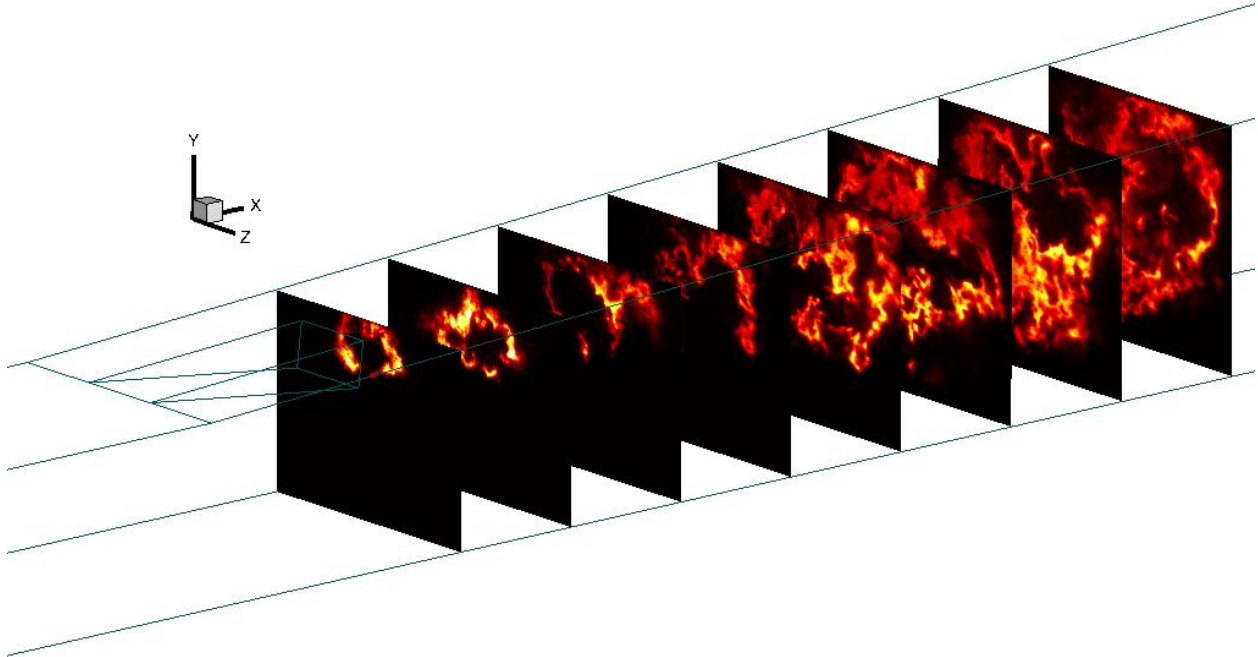


Figure 14. Combustor 3D wireframe drawing with single-shot PLIF overlay showing streamwise distribution from $x/H = 1$ to 22 for $\phi=0.49$. Configuration C.

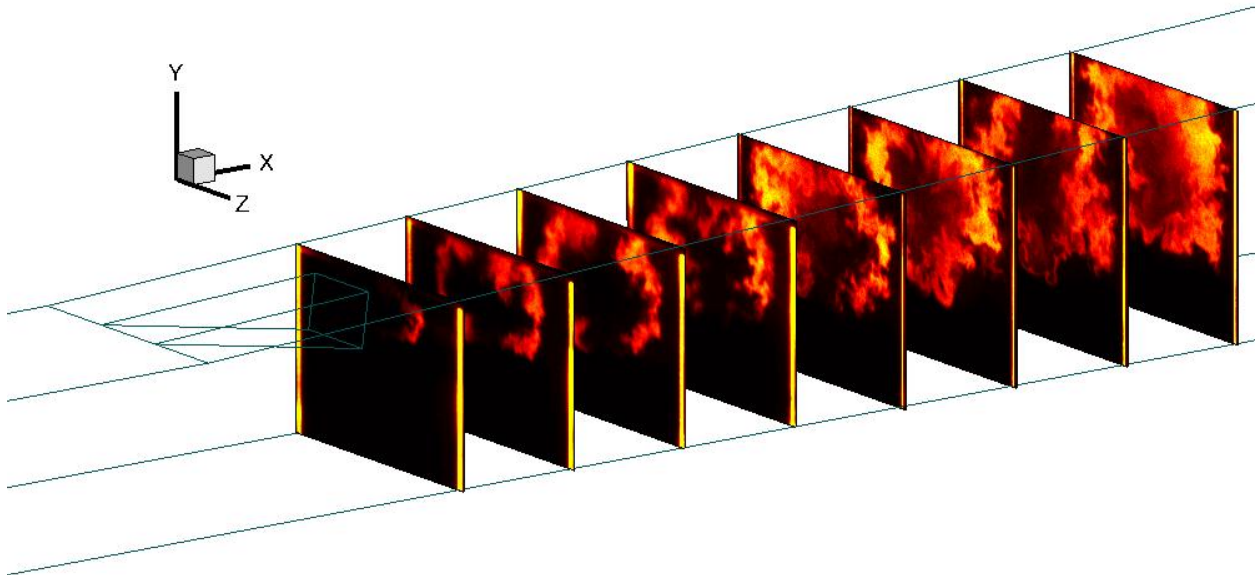


Figure 15. Combustor 3D wireframe drawing with single-shot PLIF overlay showing streamwise distribution from $x/H = 1$ to 22 for $\phi=0.17$. Configuration A. Adapted from [5].

V. Discussion

The asymmetry apparent in the results presented above, particularly for the case of lower fuel equivalence ratio, appears to be most severe at the upstream end of the combustor, towards the fuel injector. This observation agrees with results from configuration A tests where the distribution became more symmetric further downstream.⁵ CARS measurements in configuration A showed asymmetry in the temperature distribution upstream of the injector⁴ which could be attributed to non-uniform electric heating in the facility heater. Since the fluorescence signal is sensitive to the gas temperature, asymmetry in the PLIF signal could be partially caused by the temperature asymmetry observed

by CARS. Further, asymmetry in the test section geometry (compression ramp) could have an influence on PLIF signal observed.

Asymmetry can also be caused by laser absorption where a decrease in PLIF signal occurs in the laser sheet propagation direction. The effect is amplified at higher OH concentrations. However, the results show a PLIF signal gradient opposite to what would be expected from laser absorption alone. In addition, at higher equivalence ratios, it is expected that the severity of asymmetry would become worse. The PLIF results indicate that there is less asymmetry for higher equivalence ratios.

Gas velocity components in the direction of the laser sheet (z) can result in a Doppler shift. This occurs as the effective laser frequency changes when molecules travel toward or away from the laser source. Since the spectral width of the laser is narrow ($<1 \text{ cm}^{-1}$), a cross-stream Doppler shift could affect the PLIF signal and result in an asymmetric distribution. However, CFD results reported by Fulton *et al.* for configuration A indicated that cross-stream velocity magnitudes were relatively small.¹² Therefore, it is not expected that the Doppler shift caused the observed asymmetry.

Further analysis of the images showed that the orientation of the camera (camera view 1 versus 2) has an effect on the magnitude of asymmetry. Figure 16 shows a comparison of PLIF asymmetry observed at $x/H = 6$ and at an equivalence ratio of $\phi = 0.18$. While asymmetry is significant for both camera views, it is more severe for camera view 2. Quantitatively, the ratio of the peak PLIF signals corresponding to the two lobes indicates greater asymmetry in camera view 2. This effect was more apparent for configuration A, where the camera views overlapped at a position further downstream ($x/H = 12$).

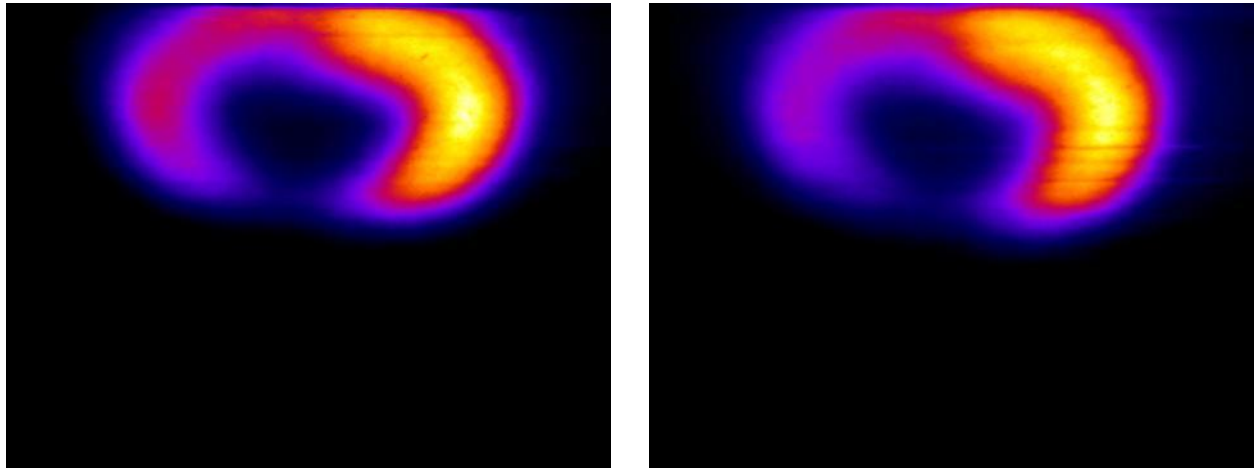


Figure 16. Asymmetry in the PLIF signal observed from camera views 1 (left) and 2 (right). Configuration C, $x/H = 6$, $\phi=0.18$.

This effect can be explained by radiative trapping. In both camera views, the camera images the laser sheet at an angle and from the side of the facility opposite the incoming laser. As a result, the total amount of OH on the optical path between the camera and laser sheet is dependent on the camera view configuration. In general, the amount of OH increases in the streamwise direction as shown in Fig. 17. If we consider a line integral of OH concentration along the two detection paths illustrated, the total integrated OH concentration will be considerably higher for path 1 as this detection path travels through more OH before reaching the CCD camera. As a result, radiative trapping will be larger in the $-z$ direction, resulting in an asymmetric PLIF image similar to those observed in Fig. 16. Even with laser absorption effects acting in the opposite direction to radiative trapping, and therefore expected to cancel out some of the radiative trapping effects, the observed asymmetry suggests that radiative trapping is more dominant than absorption.

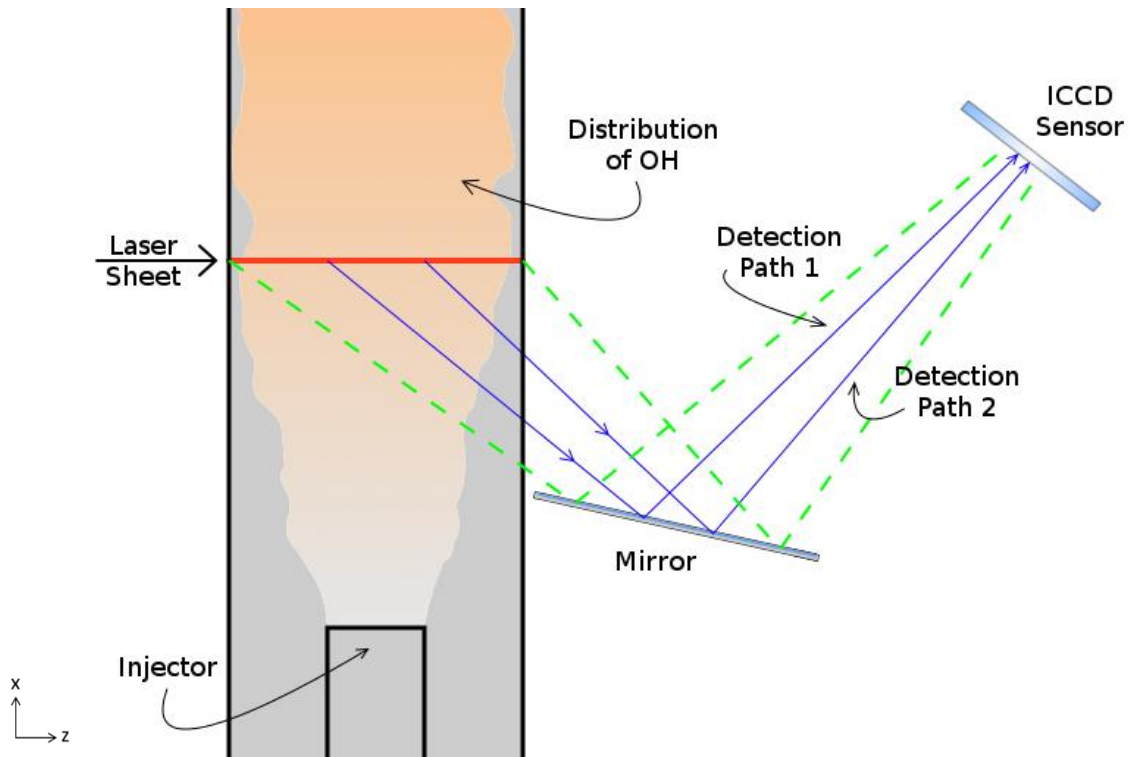


Figure 17. Illustration of OH concentration along the detection paths for camera view 1.

Figure 18 shows a schematic of the optical path for camera view 2. Similar to camera view 1, there is a larger integrated OH concentration along path 1 compared to path 2. However, because overall OH levels increase in the streamwise (+ x) direction, the radiative trapping effect that causes asymmetry is amplified in images corresponding to camera view 2. Because camera views 1 and 2 used different optical paths, the average PLIF signal intensity from overlapping streamwise positions was used to calibrate the overall intensities between the two camera views. Therefore, differences in overall signal levels associated with changes in radiative trapping between the camera views were corrected. As the laser sheet moves downstream, magnitudes of radiative trapping and laser absorption increase. However, it is likely that overall signal levels are artificially low at these downstream positions.

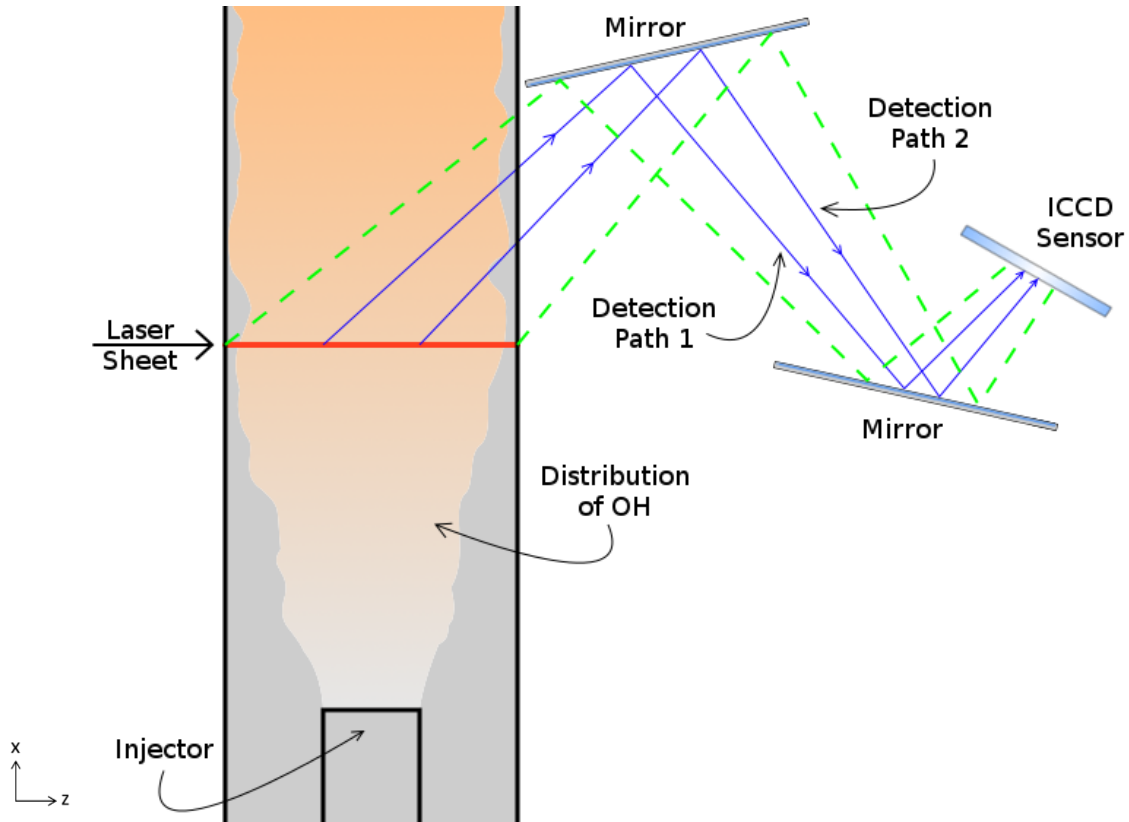


Figure 18. Illustration of OH concentration along the detection path for camera view 2.

At higher equivalence ratios, higher OH concentrations are expected at a given streamwise position. As a result, the magnitude of laser absorption is higher and can counteract the effects of radiative trapping. This would result in symmetric PLIF images, which is observed experimentally. In general, radiative trapping and laser absorption both contribute to asymmetry, but the dominant effect is a function of the concentration of OH along the optical detection path and the quantity of OH at the laser sheet location. Detailed modeling of the flow field and spectroscopic absorption effects would be required to prove these claims.

In these tests, the $Q_1(8)$ transition of OH was used due to its relative insensitivity to changes in temperature, allowing for a PLIF signal roughly proportional to local OH concentration. Unfortunately, the $(v'=1, v''=0)$ band has the drawback that for high concentrations of OH or larger dimensioned facilities there is an increase in laser beam attenuation and radiative trapping. Although it is possible to defend against these effects by exciting a weaker band $(v'=3, v''=0)$, the overall signal-to-noise ratio is expected to be lower.¹⁵

VI. Conclusions

In this paper, processed OH PLIF images obtained from the University of Virginia Scramjet Combustion Facility for configuration C have been presented. Similar to configuration A results, the fuel equivalence ratio was found to have an effect on the combustion zone shape and the turbulence structure in the flow. It is proposed that the shock wave structure in the freestream flow upstream of the compression ramp injector is sensitive to fuel flow rate and magnitude of heat release. As a result, the Mach number of the freestream flow that interacts with the compression ramp is affected, resulting in a change in the turbulence field and combustion zone shape further downstream. Through this mechanism, higher fuel equivalence ratio tests with a corresponding subsonic freestream flow near the injector result in combustion at the injector surface. In contrast, lower equivalence ratio tests with a corresponding supersonic freestream flow do not show large OH concentration levels near the injector surface. Asymmetry of OH PLIF images in configurations A and C is primarily attributed to optical density effects, including laser sheet absorption and radiative trapping, and facility flow effects. While radiative trapping and laser sheet absorption result in larger asymmetry near the fuel injector, these competing effects cause an overall reduction in PLIF signal.

Strategies to remove error from future tests due to optical density effects were discussed. The results presented contribute to the growing database for computational fluid dynamics model validation for scramjet flows.

Acknowledgements

Dr. Johansen was supported by the Natural Sciences and Engineering Research Council of Canada (NSERC). This work was supported by the AFOSR/NASA National Center for Hypersonic Combined Cycle Propulsion grant FA 9550-09-1-0611. The technical monitors are Chiping Li from the AFOSR and Rick Gaffney from NASA. We wish to thank Killian Danehy for assisting in the preliminary processing and presentation of these data.

References

¹ Rockwell, R.D., Goynes, C.P., Rice, B.E., Tatman, B.J., Smith, C., Kouchi, T., McDaniel, J.C., Fulton, J.A., and Edwards, J.R., "Close-Collaborative Experimental and Computational Study of a Dual-Mode Scramjet Combustor," AIAA-2012-113, *50th AIAA Aerospace Sciences Meeting and Exhibit*, Nashville, TN, 2012.

² Goldstein, C.S., Shultz, I.A., Jeffries, J.B., and Hanson, R.K., "Tunable Diode Laser Absorption Sensor for Measurements of Temperature and Water Concentration in Supersonic Flows," AIAA-2011-1094, *49th AIAA Aerospace Sciences Meeting and Exhibit*, Orlando, FL, 2011.

³ Busa, K.M., Bryner, E., McDaniel, J.C., Goynes, C.P., Smith, C.T., and Diskin, G.S., "Demonstration of Capability of Water Flux Measurement in a Scramjet Combustor using Tunable Diode Laser Absorption Tomography and Stereoscopic PIV," AIAA-2012-1294, *49th Aerospace Sciences Meeting and Exhibit*, Orlando, FL, 2011.

⁴ Cutler, A.D., Magnotti, G., Cantu, L., Gallo, E., Danehy, P.M., Rockwell, R., Goynes, C., McDaniel, J., "Dual-Pump CARS Measurements in the University of Virginia's Dual-Mode Scramjet: Configuration A," AIAA Paper 2012-0114, *50th AIAA Aerospace Sciences Meeting and Exhibit*, Nashville, TN, 2012.

⁵ Johansen, C.T., McRae, C.D., Danehy, P.M., Gallo, E., Cantu, L., Magnotti, G., Cutler, A., Rockwell, R., Goynes, C., McDaniel, J., "OH PLIF Visualization of the UVa Supersonic Combustion Experiment: Configuration A," AIAA Paper 2012-2887, *42nd AIAA Fluid Dynamics Conference and Exhibit*, New Orleans, LA, 2012.

⁶ Seitzman, J.M. and Hanson, R.K., "Comparison of Excitation Techniques for Quantitative Fluorescence Imaging of Reacting Flows," AIAA Journal, Vol. 31, No. 3, pp. 513-519, 1993.

⁷ Svelto, O., *Principles of Lasers*, 5th Edition, Springer, New York, 2009.

⁸ Quagliaroli, T.M., Laufer, G., Hollo, S.D., Krauss, R.H., Whitehurst, R.B., and McDaniel, J.C., "Planar KrF Laser-Induced OH Fluorescence Imaging in a Supersonic Combustion Tunnel," *Journal of Propulsion and Power*, Vol. 10, No. 3, pp. 377-381, 1994.

⁹ Laufer, G., Quagliaroli, T.M., Krauss, R.H., Whitehurst III, R.B., McDaniel, J.C., and Grinstead, J.H., "Planar OH Density and Apparent Temperature Measurements in a Supersonic Combusting Flow," AIAA Journal, Vol. 34, No. 3, pp. 463-469, 1996.

¹⁰ O'Byrne, S., Stotz, I., Neely, A.J., Boyce, R.R., Mudford, N.R., and Houwing, A.F.P., "OH PLIF Imaging of Supersonic Combustion using Cavity Injection," AIAA-2005-3357, *13th International Space Planes and Hypersonics Systems and Technologies Meeting*, Capua, Italy, 2005.

¹¹ Le, D.B., Goynes, C.P., and Krauss, R.H., "Shock Train Leading-Edge Detection in a Dual-Mode Scramjet," *Journal of Propulsion and Power*, Vol. 24, No. 5, pp. 1035-1041, 2008.

¹² Fulton, J.A., Edwards, J.R., Hassan, H.A., Rockwell, R., Goynes, C., McDaniel, J., Smith, C., Cutler, A., Johansen, C., Danehy, P.M., and Kouchi, T., "Large-Eddy / Reynolds-Averaged Navier-Stokes Simulations of a Dual-Mode Scramjet Combustor," AIAA-2012-0115, *50th AIAA Aerospace Sciences Meeting and Exhibit*, Nashville, TN, 2012.

¹³ Danehy, P.M., Alderfer, D.W., Inman, J.A., Berger, K.T., Buck, G.M., and Schwartz, R.J., "Fluorescence Imaging and Streamline Visualization of Hypersonic Flow over Rapid Prototype Wind-Tunnel Models," Proc. IMechE, Part G: J. Aerospace Engineering, 222(G5), pp. 637-651, 2008.

¹⁴ Rasband, W.S., ImageJ, U.S. National Institutes of Health, Bethesda, MD, USA, <http://rsb.info.nih.gov/ij/>, 1997-2009.

¹⁵ Quagliaroli, T.M., Laufer, G., Krauss, R.H., and McDaniel, J.C., "Laser Selection Criteria for OH Fluorescence Measurements in Supersonic Combustion Test Facilities," AIAA Journal, Vol. 31, No. 3, pp. 520-527, 1993.